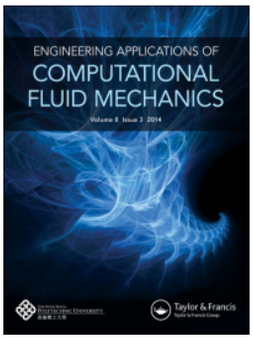

Engineering Applications of Computational Fluid Mechanics

ISSN: (Print) (Online) Journal homepage: www.tandfonline.com/journals/tcfm20

Impact of trailing-edge modification in stator vanes on heat transfer and the performance of gas turbine: a computational study

Thanh Dam Mai, Duy-Tan Vo, Byungwook Kim, Uideok Lee, Dokyun Kim, Hyoungsoon Lee & Jaiyoung Ryu

To cite this article: Thanh Dam Mai, Duy-Tan Vo, Byungwook Kim, Uideok Lee, Dokyun Kim, Hyoungsoon Lee & Jaiyoung Ryu (2024) Impact of trailing-edge modification in stator vanes on heat transfer and the performance of gas turbine: a computational study, Engineering Applications of Computational Fluid Mechanics, 18:1, 2393430, DOI: 10.1080/19942060.2024.2393430

To link to this article: https://doi.org/10.1080/19942060.2024.2393430

© 2024 The Author(s). Published by Informa UK Limited, trading as Taylor & Francis Group.

Published online: 22 Aug 2024.

Submit your article to this journal

Article views: 582

View related articles

View Crossmark data

Full Terms & Conditions of access and use can be found at
https://www.tandfonline.com/action/journalInformation?journalCode=tcfm20

ENGINEERING APPLICATIONS OF COMPUTATIONAL FLUID MECHANICS
2024, VOL. 18, NO. 1, 2393430
https://doi.org/10.1080/19942060.2024.2393430

Taylor & Francis
Taylor & Francis Group

OPEN ACCESS Check for updates

Impact of trailing-edge modification in stator vanes on heat transfer and the performance of gas turbine: a computational study

Thanh Dam Mai[a,b], Duy-Tan Vo[c], Byungwook Kim[a], Uideok Lee[a], Dokyun Kim[d], Hyoungsoon Lee[a] and Jaiyoung Ryu[e]

[a]Department of Mechanical Engineering, Chung-Ang University, Seoul, Republic of Korea; [b]Faculty of Mechanical Engineering and Technology, Ho Chi Minh City University of Industry and Trade, Ho Chi Minh City, Vietnam; [c]Department of Intelligent Energy and Industry, Chung-Ang University, Seoul, Republic of Korea; [d]Department of Mechanical and System Design Engineering, Hongik University, Seoul, Republic of Korea; [e]School of Mechanical Engineering, Korea University, Seoul, Republic of Korea

ABSTRACT

Despite extensive studies on the modification of airfoil profiles, most studies have primarily focused on the turbulent wave development and aerodynamic characteristics of modified airfoils. Moreover, studies considering the combined effects of hot-streak conditions at the turbine inlet and the modified profile of stator vanes on gas turbine performance are scarce. Thus, this study conducted a detailed numerical analysis to examine the effects of various trailing-edge (TE) profile modifications at the first stator vane on the heat transfer characteristics and performance of a high-pressure gas turbine. Four cases were investigated: a typical TE (without modification) as the reference case and three modification cases based on the wavelength number (TE-2, TE-4, and TE-8). The Reynolds-averaged Navier – Stokes equations coupled with the $k-\omega$ SST γ θ model were employed to solve the complex fluid flow through the 1.5-stage GE-E^3 gas-turbine model. The modified cases noticeably increased the heat transfer and aerodynamic characteristics of the blade/vane surface by a maximum of approximately 1–2% owing to the effects of the TE profile on the generation of the passage vortex and secondary flow. This increased the thermal and mechanical stresses, particularly in the hub and shroud regions, which may reduce the fatigue life of the blade/vane components. Furthermore, under the effects of the first stator TE profile on the tip leakage flow, the TE-2 case exhibited a slight increase in the overall efficiency (approximately 0.15%). In contrast, the efficiencies of the other modifications decreased compared to the reference case.

ARTICLE HISTORY
Received 20 November 2023
Accepted 11 August 2024

KEYWORDS
Gas turbine; trailing-edge modification; heat transfer; overall efficiency; CFD

1. Introduction

Currently, gas turbines are key components of power plants and crucial equipment in the industry because of their low weight and upfront costs (Boyce, 2011). Turbine efficiency is a critical parameter that strongly affects the output of power plants and the operation of aero-engines. In recent decades, various technologies, including materials and methods for cooling and coating, have been developed to improve the efficiency and performance of gas turbines (J. Liu et al., 2016; J. Liu et al., 2018; Prapamonthon et al., 2019; Qiao et al., 2022; Wu et al., 2022; Yao et al., 2021). Turbine inlet temperature is considered the most common and easiest method to enhance gas turbine efficiency. However, developing materials for manufacturing turbine blades and vanes is challenging. Recently, gas turbines have been designed to operate at high temperatures (approximately 1900K; Mishra et al., 2020) to satisfy high-efficiency requirements. This critical environment results in a high thermal load and temperature gradient on the blade and vane surfaces, resulting in damaged or even broken or failed blades. Therefore, studies that provide accurate predictions of heat transfer characteristics in the gas turbine stage are critical.

The combustor exit conditions significantly affect the aerodynamic efficiency and thermal performance of gas turbines in aero-engines. Previous studies (Y. Jiang et al., 2018; Zeng et al., 2018) applied a uniform combustor exit for the gas turbine inlet, providing valuable insights related to the development of gas turbine designs. However, the gas turbine inlet is non-uniform during operation, with a substantial temperature variation in the radial and circumferential directions (T Povey et al., 2007; Thomas Povey & Qureshi, 2009). This temperature variation is referred to as a hot-streak. Hot streaks have a significant impact on the heat transfer characteristics of high-pressure turbine rotor blades, leading to a critical rise in thermal loading on the pressure

CONTACT Hyoungsoon Lee leeh@cau.ac.kr; Jaiyoung Ryu jryu@korea.ac.kr

© 2024 The Author(s). Published by Informa UK Limited, trading as Taylor & Francis Group.
This is an Open Access article distributed under the terms of the Creative Commons Attribution-NonCommercial License (http://creativecommons.org/licenses/by-nc/4.0/), which permits unrestricted non-commercial use, distribution, and reproduction in any medium, provided the original work is properly cited. The terms on which this article has been published allow the posting of the Accepted Manuscript in a repository by the author(s) or with their consent.

surfaces. This phenomenon, commonly referred to as 'preferential heating,' has been extensively documented in both experimental and computational studies (Butler et al., 1989; Dorney et al., 1992). Preferential heating occurs when there is an enhanced cross-passage flow of hot gas from the suction to the pressure surface within the hot region of the fluid, resulting from an increased incidence angle. This mechanism can be likened to the phenomenon observed in wakes shed from vanes and convected into downstream rotating rows, albeit with an opposite behaviour. In this case, a decrease in incidence angle caused by the velocity deficit facilitates the convection of wakes from the pressure to the suction side of the blade (Kerrebrock & Mikolajczak, 1970).

The nonuniformity of the turbine inlet has been described in various forms, such as radial, rounded, and elliptical distributions. Consequently, it has been proposed that a higher temperature is usually located at the mid-span. By contrast, lower temperatures are distributed around the hub and shroud regions (An et al., 2009; He et al., 2007; Saxer & Giles, 1993). In addition, hot-streak conditions significantly influence the thermal efficiency and aerodynamic behaviour of high-pressure gas turbines. Beard et al. (Beard et al., 2013) conducted an experimental and numerical study on the effects of uniform and nonuniform turbine inlet temperatures on turbine efficiency and reported a decrease in turbine efficiency under hot-streak conditions. In addition, Simone et al. (Simone et al., 2012) conducted a numerical analysis of the effects of hot-streaks on the heat transfer and fluid flow in high-pressure gas turbines. They reported an increase in the heat transfer rate on the nozzle guide vanes under hot-streak conditions compared with a uniform inlet temperature.

Recently, Mansouri (Mansouri, 2021) conducted unsteady simulations to investigate the flow and heat transfer in the gas turbine stage under various hot-streak conditions. A significant increase in the heat transfer characteristics on the suction side (SS) of rotor blades was observed owing to the effects of vortices. Therefore, the hot-streak conditions must be considered in gas turbine research to improve the comprehensive knowledge of aero-engine design. Energy loss through the gas turbine stage significantly affects its efficiency and performance. Therefore, reducing the energy loss through the gas turbine stage is economically useful. Moreover, fuel consumption decreases significantly with energy loss reduction owing to the continuous operation of gas turbines in aero-engines.

The modification of turbine blades and vanes is among the best methods to reduce energy loss (Chen et al., 2020) and improve the efficiency and performance of turbomachinery equipment. Kaewbumrung et al. (Kaewbumrung et al., 2019) proposed a numerical investigation of a trailing-edge (TE) modification with a blended method on the aerodynamic behaviour of a compressor blade. The aerodynamic characteristics were found to improve after repair. Mai and Ryu (2020, 2021) simulated the effects of leading-edge modification at various locations of damaged rotor blades on the heat transfer characteristics, efficiency, and thermal loading on the blade and vane surfaces in a high-pressure gas turbine. Consequently, the efficiency was enhanced after modification; however, the heat transfer coefficient (HTC) and thermal loading increased significantly around the damaged locations and rotor blade tips. Luo et al. (2021) conducted a numerical analysis of the effects of a biomimetic TE on the energy loss through a high-pressure gas-turbine stage. They reported a significant decrease in the energy loss at this stage. Thus, this study considered the influence of various TE modifications on high-pressure gas turbine efficiency and aero-thermal characteristics. The results of this study provide useful information regarding the effects of the transformation of blade/vane profiles on gas turbine efficiency during design activities.

A numerical analysis of the complex fluid flow and heat transfer characteristics in high-pressure gas turbines must be conducted within a multistage domain to facilitate accurate predictions. Moreover, it should match the actual conditions during the operation. However, gas turbine simulations within the multistage domain are costly and sometimes exceed the computational limits. Therefore, the number of stages used for the simulations must be considered to ensure rigorous prediction with sufficient calculation time and cost. Because of this consideration, previous studies (Pogorelov et al., 2019; Wang et al., 2016; B. Zhang & Qiang, 2021) have performed simulations considering only one stage of the gas turbines. These studies claimed that the simulated results were consistent with experimental data, although only a single-stage gas turbine was used. In addition, hot-streak conditions strongly influence fluid flow and heat transfer in the first stage of a gas turbine. Thus, in this study, we considered the coupled effects of hot-streaks and modifications at the TE of the stator profile. Therefore, we selected a 1.5-stage gas turbine in the computational domain. This consideration is consistent with recent studies on gas turbines (Li et al., 2019; Mai & Ryu, 2020, 2021). Moreover, we must consider the simulation type (steady or transient) that ensures accurate results for the computational model. Schmid et al. (2014) reported that the gas turbine efficiency under unsteady simulations differed from that under steady simulations, indicating that transient simulations could accurately predict the gas turbine performance after simulating a 1.5-stage gas turbine. In this study, we considered a 1.5-stage gas turbine

to conduct transient simulations to investigate the combined effects of hot-streak conditions and profile modifications on the aerothermal characteristics and efficiency of a high-pressure gas turbine.

Various studies on the modification of airfoil profiles have been proposed (Luo et al., 2021; Mai & Ryu, 2020, 2021; Yan et al., 2021). However, previous studies primarily focused on the turbulent wave development and aerodynamic characteristics of modified airfoils. Limited research has considered the combined effects of hot-streak conditions at the turbine inlet and the modified profile of stator vanes on gas turbine performance. Therefore, this study proposed a numerical analysis of the overall efficiency and aerothermal behaviour in the first 1.5-stage of GE-E^3 high-pressure gas turbines, emphasising the combined effects of hot-streak conditions on various types of modified stator vanes. The Reynolds-averaged Navier – Stokes method was applied to the transient simulations to examine the complex fluid flow in the gas turbine stage. The energy losses were analyzed and discussed. Consequently, the overall efficiency was presented with a detailed fluid flow analysis and heat-transfer characteristics. Furthermore, the results of this study can provide useful knowledge regarding the effects of profiled modifications on gas-turbine performance, which should be noted during the design period.

2. Computational model and boundary conditions

2.1. Computational model and grid

The first 1.5-stage geometry of the GE-E^3 gas turbine was used in the computational domain. It was extracted from a NASA report (Timko, 1984) and was widely used in various numerical studies (Choi & Ryu, 2018; Kwak & Han, 2003; J.-J. Liu et al., 2013). The original geometry included 46 and 48 vanes for the first and second stators, respectively, and 76 rotor blades. The pitch angles between the stator and rotor should remain constant for unsteady simulations to ensure accurate prediction results and minimise calculation time. The domain scaling method (Arnone & Benvenuti, 1994) was used to satisfy this requirement. Domain scaling is a computational technique utilised in turbomachinery simulations to streamline the computational domain. This method involves modifying the number of blades or vanes to ensure that the blade-to-vane ratio corresponds to the ratio of two small integers (such as 1/1, 1/2, 1/3, 2/3, etc.) while preserving the airfoil's shape. This method was implemented to scale the first and second stator-vane domains, employing scale ratios of 46/38 and 48/38, respectively. Previous studies included more details about the scaling for the computational domain and blade and vane dimensions (Choi & Ryu, 2018; Mai & Ryu, 2020, 2021). The final numbers of the first stator vanes, rotor blades, and second stator vanes were determined to be 38, 76, and 38, respectively. These figures closely align with those reported in previous studies (S. Jiang et al., 2023; Z. Liu et al., 2014; B. Zhang et al., 2020), ensuring consistency and comparability in our analysis. During the application of the domain scaling technique, the vane was enlarged by a factor of 1.21 compared to the original, while the pitch ratio remained unchanged. This configuration was additionally similar to recent studies (Du et al., 2016; Z. Liu et al., 2014; Xu et al., 2018; B. Zhang et al., 2019). This study focused on four types of first-stator vanes: one typical and three modified vanes. The modified cases had the same depth ($d = 0.01c$), where c is the chord length of the first stator vane ($c = 85.21$ mm) (Choi & Ryu, 2018). The difference between the modified cases was in wavelength numbers: two, four, and eight. The formulation employed to describe the modification made to the stator trailing edge was as follows:

$$f(x) = \frac{d}{2}\sin\left(\frac{2\pi}{\lambda_i}x\right), \tag{1}$$

where $f(x)$ is the function describing the wavelengths along the stator trailing-edge;

d is the depth of wavelength;

c presents the chord length of the first stator;

λ_i is the wavelength depending on the number of wavelengths along the stator trailing-edge i ($\lambda_i = \frac{h}{i}$);

h denotes the height of the stator trailing-edge;

x presents the location along the stator trailing-edge.

Figure 1(a–d) shows the detailed computational domain and various types of TE of the first-stator vanes.

Ansys Turbogrid was utilised to generate a mesh for the computational domain. This study used a geometry similar to that of GE-E^3 gas turbines (Choi & Ryu, 2018; Mai & Ryu, 2020, 2021). Achieving an optimal mesh involves ensuring critical areas are well-resolved while maintaining computational efficiency, often through adaptive mesh refinement and grid independence studies. This study systematically evaluated the independent test mesh by comparing area-averaged heat flux and pressure on the blade/vane surfaces across various mesh qualities. Table 1 provides detailed specifications of the independent test mesh for all vanes and blades within the computational domain, with four mesh cases for each component.

For the grid independence test, grids for each blade were scaled 1.6 times based on the initial mesh dimensions. Ten prismatic grid layers were constructed near the walls with a growth rate of 1.2, and the first layer had a thickness of 5×10^{-7} m. The number of layers, the first

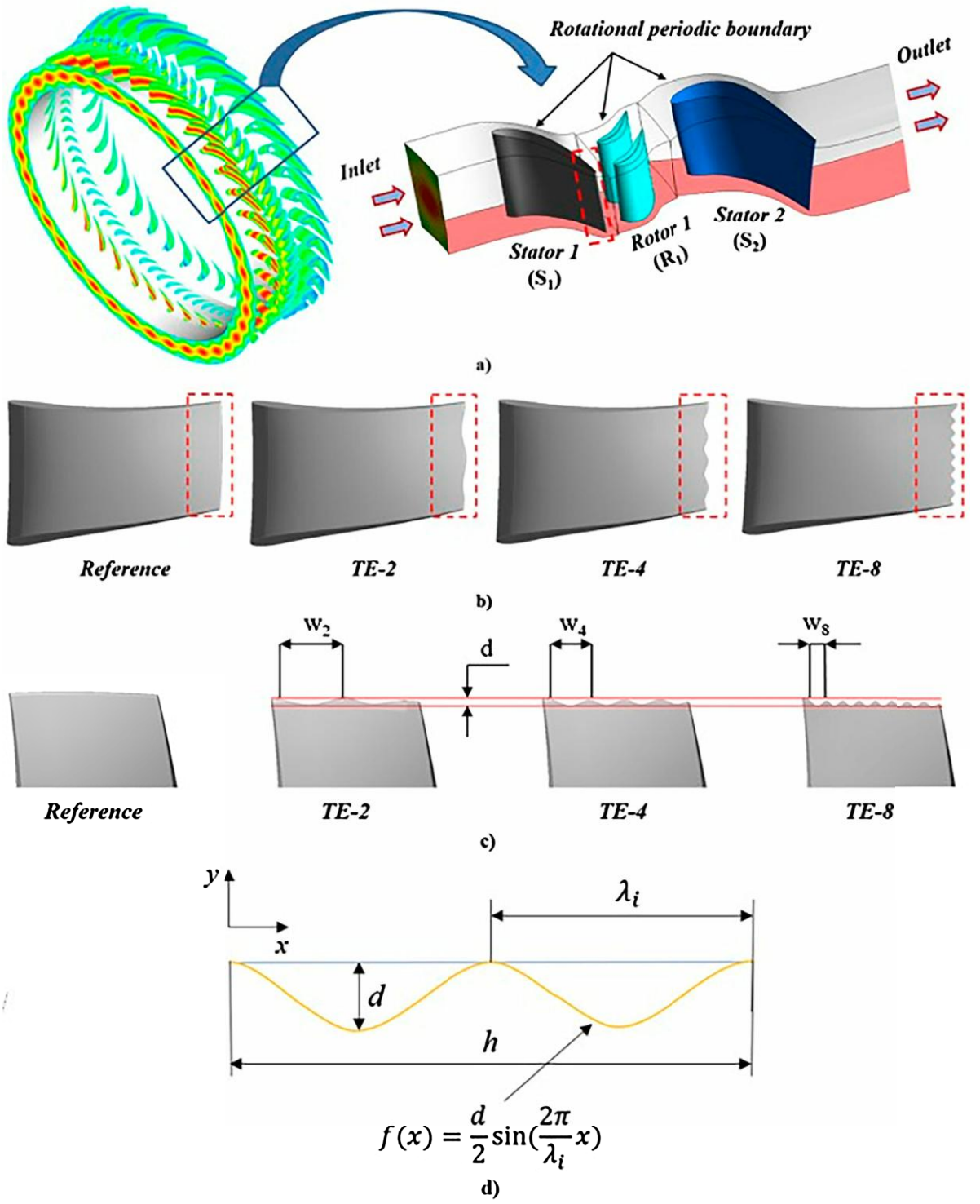

Figure 1. (a) Computational domain with full-scale geometry and simplified domain for simulations; (b) various types of Stator Vane 1; (c) side view of various types of Stator Vane 1; TE: trailing edge; 2, 4, and 8 = wavelengths along the trailing edge of S_1 vane. All waves have the same depth of 0.01*c*, where *c* is the chord length of Stator Vane 1 ($c = 85.21$ mm) (Choi & Ryu, 2018); (d) The formulation for modified stator trailing-edge.

layer thickness, and the growth rate of the prismatic grids were kept consistent across the four meshes to ensure the same level of boundary layer discretization accuracy. The selection process was based on minimising differences in area-averaged heat flux and pressure, with a tolerance of approximately 0.5%. Ultimately, a mesh with around nine million elements was selected for the computational domain.

Table 1. Independent grid test of the computational domain.

	Domain node number ($\times 10^6$)			Area-averaged heat flux (kW/m^2) *(relative error)*			Area-averaged pressure (kPa) *(relative error)*		
	S_1	R_1	S_2	S_1	R_1	S_2	S_1	R_1	S_2
Case 1	1	2.48	1.34	310.98 *(1.05%)*	370.23 *(0.93%)*	276.93 *(0.97%)*	275.28 *(1.27%)*	185.43 *(1.12%)*	127.28 *(0.95%)*
Case 2	**1.6**	**3.97**	2.14	***314.25 (0.49%)***	***373.71 (0.43%)***	279.64 *(0.47%)*	***278.78 (0.52%)***	***187.53 (0.48%)***	128.50 *(0.52%)*
Case 3	2.56	6.35	**3.43**	315.79 *(0.52%)*	375.32 *(0.45%)*	***280.96 (0.46%)***	280.23 *(0.54%)*	188.43 *(0.51%)*	***129.17 (0.45%)***
Case 4	4.09	10.16	5.49	317.43	377.02	282.26	281.740	189.40	129.75

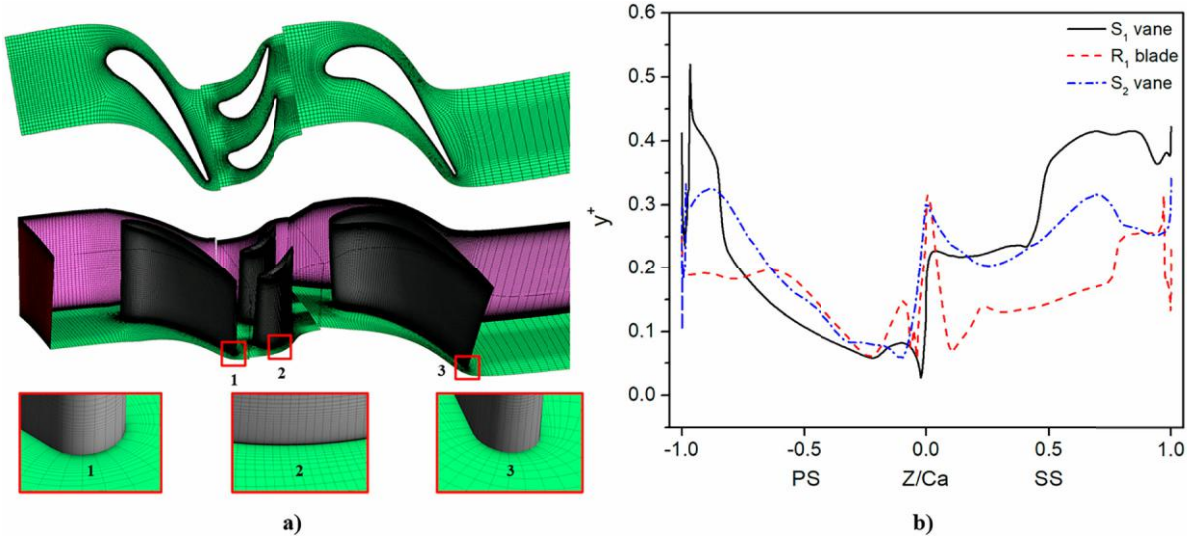

Figure 2. Mesh details for the computational domain and y^+ values along the mid-span of the vanes and blade; PS: pressure side; SS: suction side.

Figure 2 illustrates the detailed mesh configuration of the computational domain, featuring increased refinement near the blade/vane surface. Furthermore, the distribution of y^+ values along the midspan of the blade/vane surface is presented for both the pressure side (PS) and the suction side (SS). These y^+ values were maintained at approximately 0.5 to ensure an accurate prediction of flow and heat transfer near the blade/vane surface.

2.2. Numerical details and boundary conditions

This study used a commercial computational code based on the Reynolds-averaged Navier – Stokes equations and the finite volume method, ANSYS CFX, to conduct transient simulations to investigate the complex flow and heat transfer characteristics of a 1.5-stage high-pressure gas turbine. The total energy equation was used to analyze the heat transfer characteristics. A high-resolution scheme was used for the turbulence numeric and advection schemes, which considered the second-order option in sharply graded regions and changed to the first-order option in low-gradient areas. The frozen-rotor model was applied to the stator – rotor interface while conducting a steady simulation. Further, the transient rotor – stator condition was employed for the interface between the stator and rotor during unsteady simulations, wherein steady simulation results were used as the initial condition. The time step for one pitch, that is, the time required for a single rotor blade to pass through a stator passage, was carefully considered to ensure the accuracy of the simulations. We adopted a widely recognised approach to determine the optimal pitch count for the simulations. This method involved selecting specific points close to the surfaces of the blades and vanes to assess the periodic conditions of pressure and temperature. The suitability of pitch counts was established when the measured values at these designated points exhibited periodic behaviour. Throughout our study, we closely monitored the pressure and temperature values at these selected points during the initial simulations. In addition, previous studies (Choi & Ryu, 2018; Mai & Ryu, 2020, 2021; Wang et al., 2017) concluded that 32 time steps with 50 sub-iterations for one pitch were suitable for accurately predicting high-pressure gas turbines. The simulations were considered convergent when the values of the residuals of the continuity, momentum, energy, turbulent eddy dissipation equation, and turbulent kinetic energy were less than

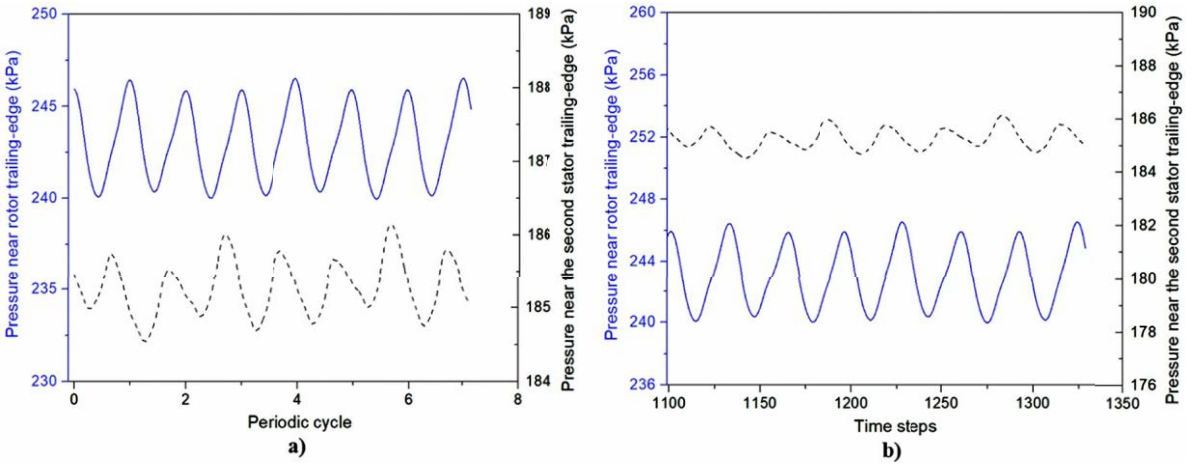

Figure 3. Convergence history of the unsteady simulation based on: (a) Clark's method and (b) the number of time steps during unsteady simulation.

10^{-6}. We also considered Clark's method (Arnone & Pacciani, 1996) to ensure the convergence of our simulation. Two monitoring points near the trailing edge of the rotor and the second stator were used to check the pressure at these locations. One periodic cycle consisted of 32 sampling values, and the results were consistent with our previously presented data. The convergence history of the unsteady simulation is shown in Figure 3.

To ensure the accuracy of the simulations under high-pressure and high-temperature conditions in the gas turbine stage, the turbulence model should be carefully specified. Each turbulence model was developed to solve specific problems. Previous studies (Abdelmaksoud & Wang, 2020; Du et al., 2016; S. Jiang et al., 2023; Z. Liu et al., 2014; Z. Liu et al., 2015; Xu et al., 2018; B. Zhang et al., 2020; B. Zhang et al., 2019) concluded that the k-ω turbulence model is suitable for simulating fluid flow passing vanes because owing to its robust nature and faster convergence than other models. Moreover, previous studies (Choi & Ryu, 2018; Mai & Ryu, 2020, 2021) have indicated that the SST k-ω with the transitional modification (γ) turbulence model is suitable for predicting the complex fluid flow and heat transfer characteristics in the gas-turbine stage. Wang et al. (2018) conducted simulations using various turbulence models to validate the experimental results of the C3X vane (Hylton et al., 1988). Their results concluded that the SST k-ω-γ -θ model provides more accurate predictions for temperature and heat flux than the pure SST k-ω model. These conclusions are similar to those reported in previous studies (Adams et al., 2021; Vo et al., 2022; S. Zhang et al., 2023). Therefore, we selected the SST k-ω with the transition formulation (γ -θ approach) turbulence model to ensure accurate simulation results.

The boundary conditions used in this study were similarly defined using a NASA report (Timko, 1984) and previous studies (Choi & Ryu, 2018; Mai & Ryu, 2020, 2021). The working fluid was considered an ideal gas. The inlet condition was set at a pressure of 344,740 Pa, with hot-streak conditions for the temperature field (maximum of 839 K and average of 728 K). The outlet condition was defined as a static pressure of 104,470 Pa. The rotational speed of the rotor was 3600 rpm. An adiabatic wall condition was applied to the blade/vane surface to investigate the temperature distribution. Isothermal conditions were used to calculate the heat transfer characteristics of the blade/vane surface (applying a constant temperature of 389.95 K). The interface between the blades and vanes was set as a frozen condition during steady simulations and as a transient rotor – stator for unsteady simulations. Furthermore, the computational time for the unsteady simulations was approximately 80 h.

2.3. Validation

To determine the most suitable turbulence model for our computational domain, we conducted simulations employing various turbulence models, including k-ε, RNG k-ε, k-ω, k-ω SST γ , and k-ω SST γ θ. This investigation aimed to identify the turbulence model best suited for studying the heat transfer characteristics in gas turbines. The numerical model used for validation was based on the work of Hylton et al. (1988), where NASA's internally film-cooled C3X vane was utilised to assess the reliability of our proposed turbulence model for investigating the flow behaviours and heat transfer characteristics.

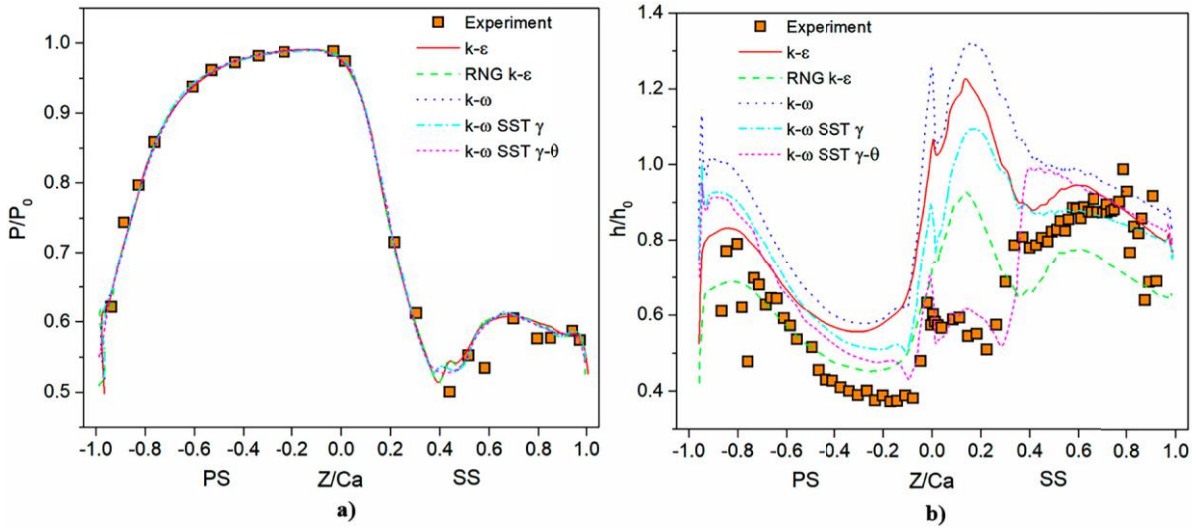

Figure 4. Comparisons of the simulation and experimental results (Hylton et al., 1988) over the mid-span of the C3X vane: (a) normalised pressure ($P_0 = 207.33$ kPa) and (b) normalised heat transfer coefficient ($h_0 = 1135\ \mathrm{W/m^2 \cdot K}$).

Experimental data from run #34145 in Hylton et al.'s study were compared with our numerical results. The mainstream inlet conditions were set at a pressure of 306.35 kPa and a temperature of 703 K, with a turbulence intensity of 6.5%. The pressure exit was 212.93 kPa, and the Mach number exit was 0.74. Ten cooling holes were distributed along the radial direction of the vane, providing cooling air with varying temperatures and flow rates. Further details regarding the boundary conditions for cooling air were varied based on hole locations, as outlined in Hylton et al. (1988).

Our simulation results exhibited trends consistent with experimental findings (Figure 4). Notably, the SST k-ω-γ -θ turbulence model demonstrated the most accurate predictions. Although discrepancies occurred in the 40–70% axial chord length regions on the pressure side (PS) and suction side (SS), the model exhibited good agreement in other regions, particularly around the trailing edge (TE). Therefore, we are confident in our numerical computation settings, which provided accurate predictions of the fluid flow complexity and heat transfer characteristics within the high-pressure gas turbine stage.

3. Results and discussion

3.1. Fluid flow characteristics

Visualising the generation of secondary flows is essential for visualising the complex fluid flow passing through the turbine stage, significantly affecting stage loss and influencing the thermal stress on the blade/vane surface. Figure 5 illustrates a three-dimensional flow structure passing through the turbine stage under hot-streak conditions at the inflow. The contours provide an overview of the core vortices generated during the turbine stage. Passage, horseshoe, and leakage vortices were formed during the movement of the complex fluid flow passing through the blade/vane surface. This section presents an analysis of the effects of various TE conditions on the flow field. Subsequently, the influences on efficiency and aerothermal characteristics are presented and discussed.

Figure 6(a) depicts the flow vorticity immediately after the modified location of the S_1 vane, aimed at assessing the impact of various TE profiles on flow characteristics. Notably, the modified cases exhibit higher vorticity levels than the reference case, attributed to changes in the TE profiles, particularly at the modified location. To facilitate a more detailed analysis, the vorticity at various span-wise locations on the surface immediately post-modification is presented in Figure 6(b). It is evident that the vorticity under the modified cases exceeds that of the reference case by approximately 10% at locations following the modification while maintaining nearly similar levels at other locations.

Furthermore, Figure 7 illustrates the effects of the modified TE profile on turbulence kinetic energy (TKE) at various span-wise locations on the surface immediately post-modification. The TKE values under the modified cases surpass those of the reference case across all locations, indicating the influence of TE profiles on flow characteristics, particularly with regard to vortex flow and turbulence intensity. The discernible difference induced by the modified location extends to approximately 40% of the dimensionless distance between two stators; subsequently, it becomes consistent across all cases. This observation leads to the conclusion that TE profile modification exerts a more pronounced effect at near-wall locations than the main stream flow. This discrepancy

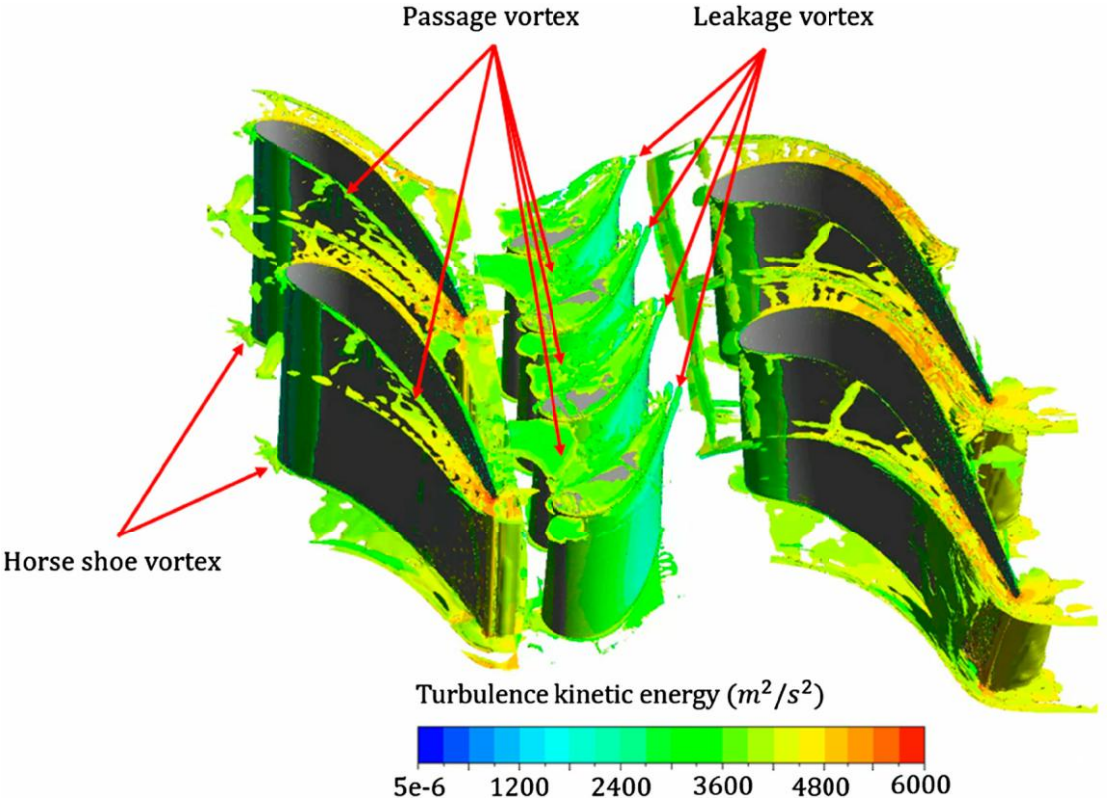

Figure 5. Instantaneous view of secondary flows through gas turbine stage; contour level is coloured according to turbulence kinetic energy.

is anticipated to significantly impact flow characteristics and heat transfer downstream. The underlying conditions arise from the modification in the TE profile, specifically linked to TE loss under the influence of changing TE thickness during modification. TE-2 reduced the TE thickness more significantly than the other modified cases (TE-4 and TE-8). Consequently, the TE loss in the modified cases was lower than that in the reference case, whereas the case of TE-2 performed best with the lowest TE loss. These results were consistent with previous studies (J. Denton & Xu, 1990; J. D. Denton, 1993). The TE profile significantly affected the downstream flow field, which strongly influenced the heat transfer characteristics on the blade/vane surface and the overall efficiency of the gas-turbine stage.

Because of the complex flow structure generated inside the vane passage and the effects of various vane conditions, the flow pressure changed significantly when it passed through the first vane. In addition, the loss owing to the effect of secondary flow is a major factor that directly affects the efficiency and overall thermal load on the blade/vane surface. Among the most popular parameters for examining the flow loss passing through a vane surface is the pressure coefficient (C_p), which is expressed as follows:

$$C_p = \frac{P_{0,\text{in}} - P_{0,\text{out}}}{P_{0,\text{in}}}, \tag{2}$$

where C_p is the pressure coefficient, $P_{0,\text{in}}$ is the stagnation pressure at the inlet, and $P_{0,\text{out}}$ is the stagnation pressure at the outlet.

Figure 8 shows the flow pressure coefficients at the interface of S_1 and R_1 for different types of S_1 TEs. The pressure coefficient of the modified S_1 vane cases was more significant than that of the reference case, owing to the effects of the TE profile on the main and secondary flows. The difference was primarily between the midspan and the region near the casing. All the modified vane cases yielded a larger pressure coefficient at the midspan owing to the effects of the main flow. However, the modified vane cases had lower pressure coefficients near the casing regions owing to the secondary flow generation (tip leakage flow), except for TE-2. This condition affected the pressure on the main flow and influenced the generation of tip leakage flow.

Figure 9(a) shows the area-averaged pressure on PS and SS on the R_1 blade surface to evaluate the effects of various TE types on S_1 vanes in the pressure field.

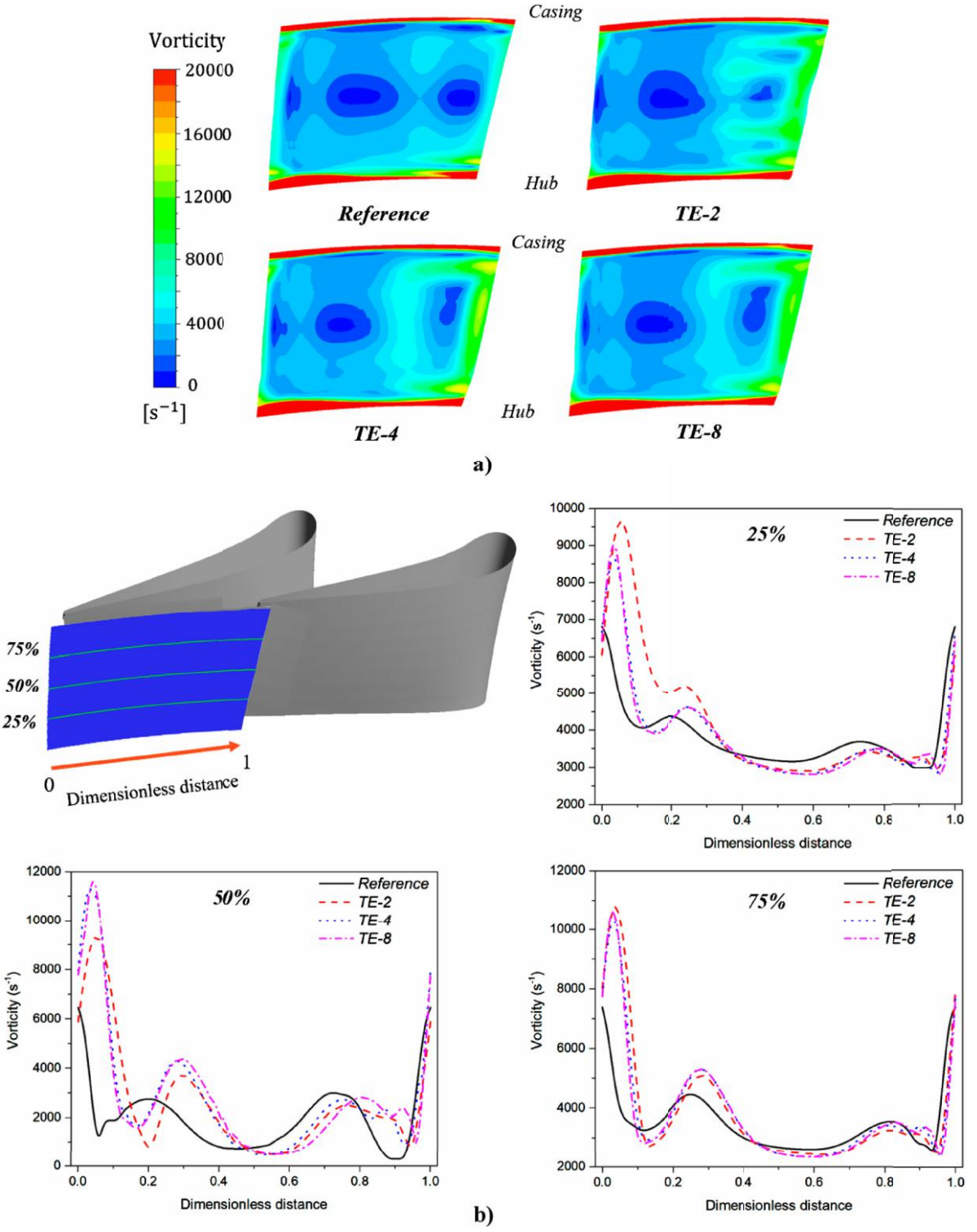

Figure 6. (a) Vorticity contour immediately after the modified location of the S_1 vane; (b) Line plots of vorticity at various span-wise locations under various types of the S_1 vane.

The pressures on PS and SS of R_1 increased owing to the higher pressure coefficient, as shown in Figure 8. This condition significantly affected the generation of secondary flows, particularly the tip leakage flow, which strongly affected the efficiency and aerothermal characteristics in the gas-turbine stage. Figure 9(b) shows the pressure difference between the PS and SS of the R_1 blade and displays the tip leakage flow passing through the

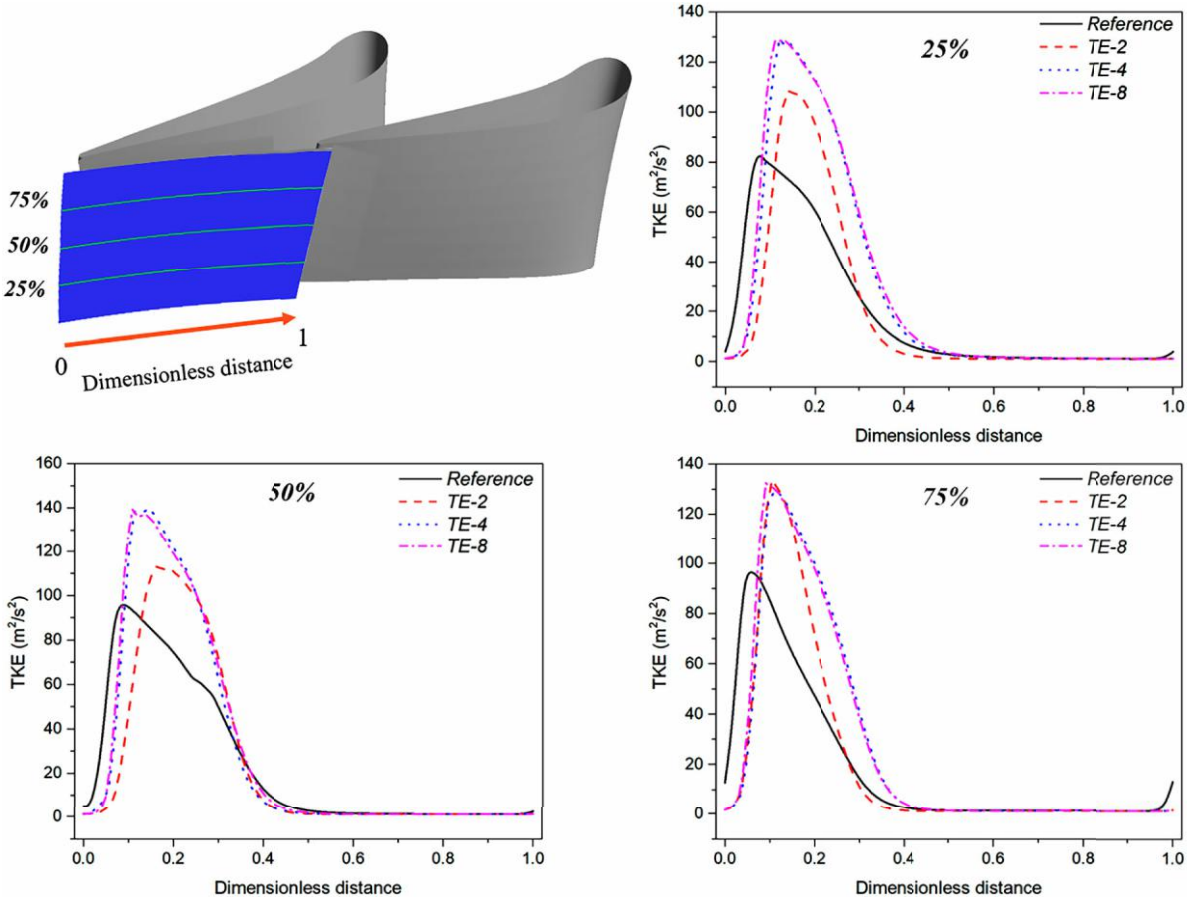

Figure 7. Turbulence kinetic energy (TKE) distribution at different locations under various types of the S_1 vane.

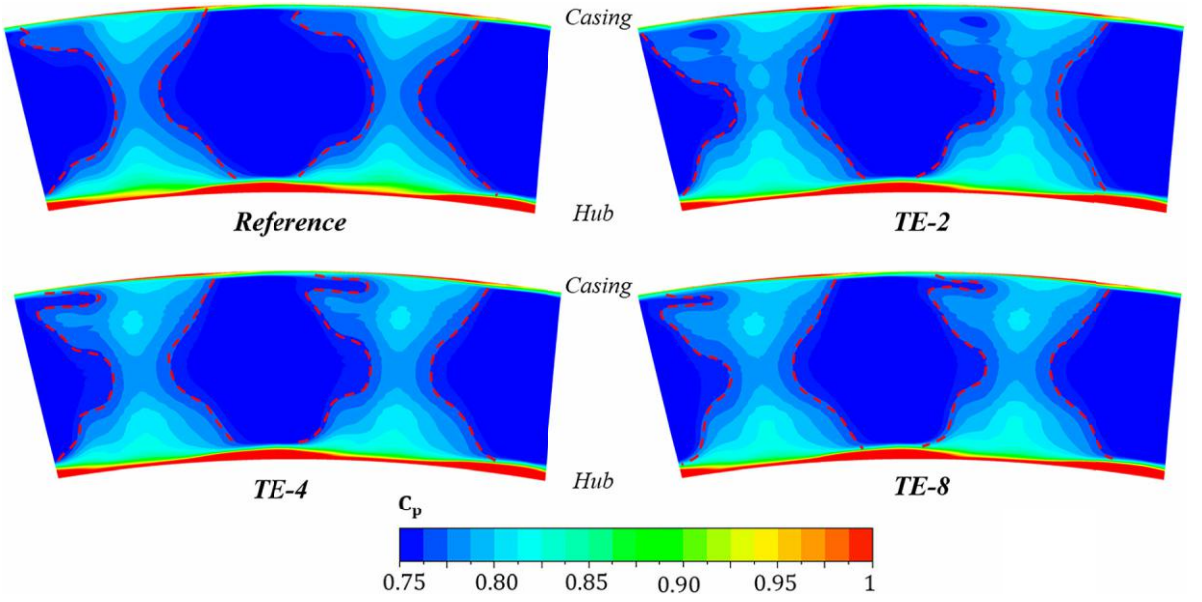

Figure 8. Pressure coefficient at the interface between the S_1 vane and R_1 blade under various types of the S_1 vane.

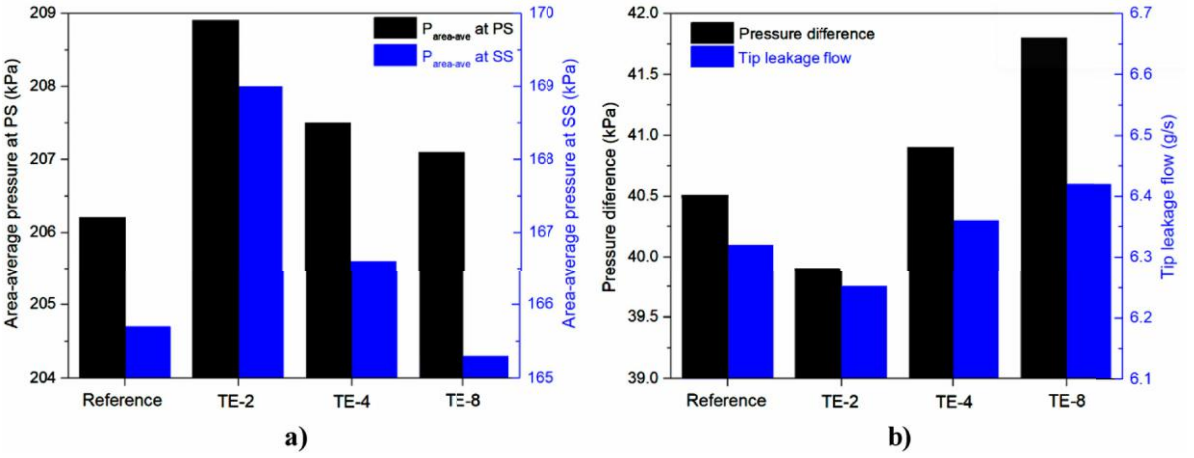

Figure 9. (a) Area-averaged pressure over the R_1 blade surface (b) Relationship between pressure and tip leakage flow over blade tip under various cases of S_1 vane trailing edge.

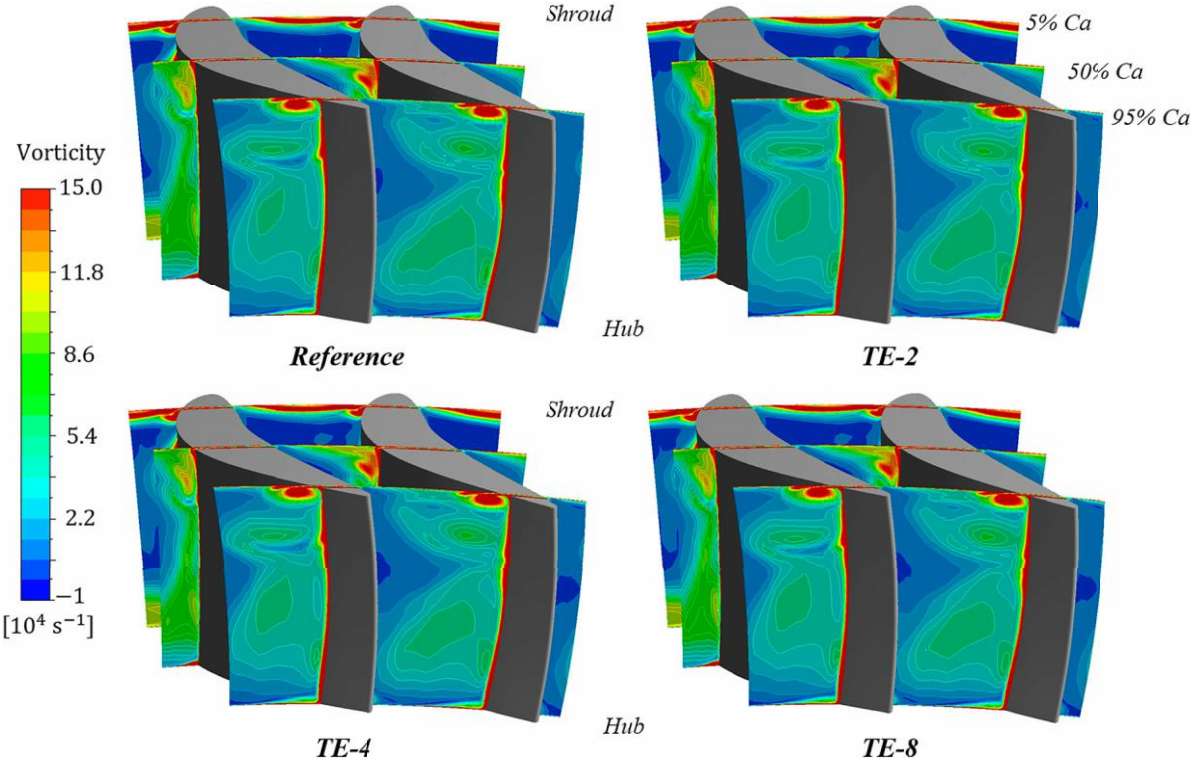

Figure 10. Flow vorticity contours at various plane surfaces along the axial chord length of the R_1 blade.

rotor blade tip. This indicated that the stator TE profile significantly affected the tip leakage flow. TE-2 exhibited the smallest leakage flow because it had the lowest pressure difference. The other modified cases (TE-4 and TE-8) exhibited greater leakage flow than the reference cases. These results are consistent with those shown in Figure 8.

Figure 10 illustrates the flow vorticity at various planes along the axial chord length of the R_1 blade, offering a detailed analysis of the impact of different stator trailing edge (TE) profiles on flow characteristics. Notably, negligible effects were observed among the cases around the hub region. However, a prominent vortex was identified along the axial chord length in the shroud region, attributed to secondary flows. At 5% Ca, a pronounced vortex near the blade tip's suction side was evident, stemming from the tip leakage flow and the leading-edge vortex as the flow traversed the blade's leading edge. Consequently, high-vorticity regions extended from the suction side to the passage.

Conversely, at 50% Ca, a reduced vortex intensity was observed compared to 5% Ca; nevertheless, the vortex

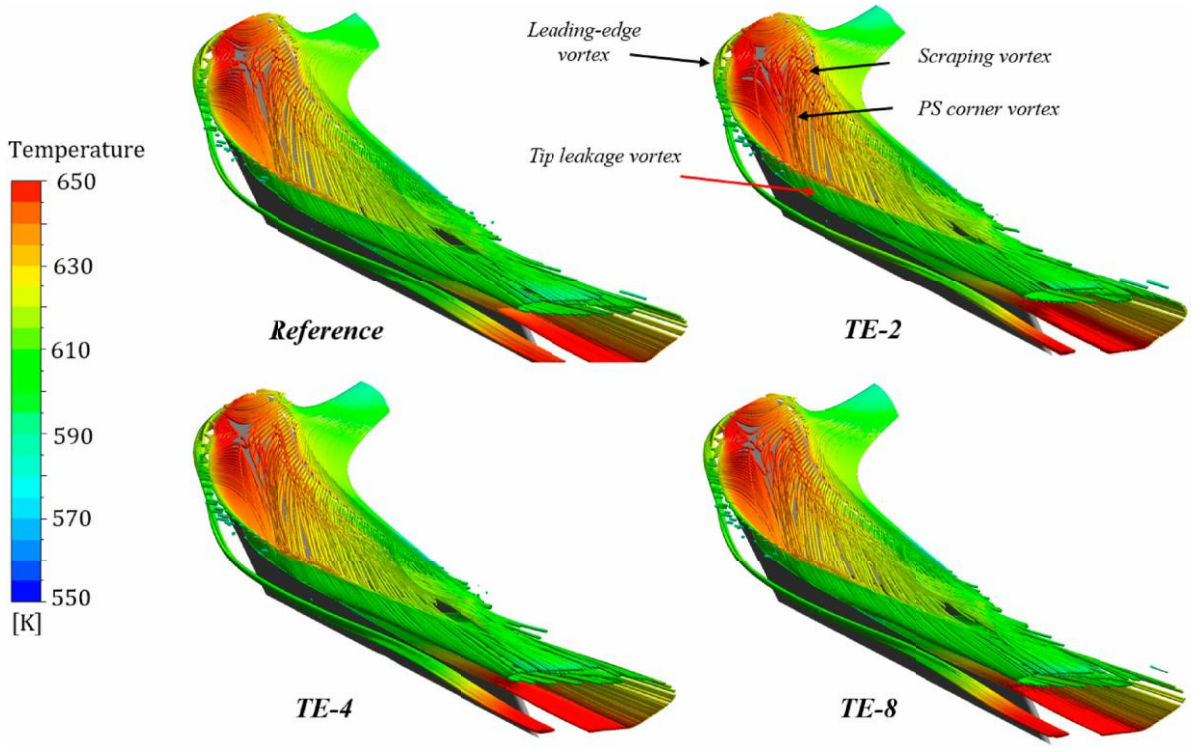

Figure 11. 3D streamlines of secondary flow distribution over the R_1 blade tip under various S_1 vane conditions.

regions were more expansive and developed along the suction side due to the amalgamation of the tip leakage vortex originating from this region with the pressure side (PS) corner vortex. In the near-trailing edge region (at 95% Ca), the high-vortex region was predominantly concentrated on the suction side around the blade tip. This concentration occurred as this region primarily retained the tip leakage vortex.

Figure 11 offers a detailed examination of the generation and evolution of vortices in the blade tip region across different S_1 vane configurations. Notably, TE-2 exhibited an exceptionally intense vortex region extending from the leading edge to approximately 30% Ca. This phenomenon is known to significantly influence the heat transfer characteristics in the vicinity, potentially resulting in a sudden escalation of heat flux. Such elevated heat flux levels have the potential to adversely impact the fatigue life of the component at these specific locations.

Figure 12 presents the contour of the total pressure loss coefficient (ζ) shown in Equation 3 to provide an insight analysis of the aerodynamic characteristics under various S_1 vane conditions:

$$\zeta = \frac{P_{ti} - P_{tl}}{\frac{1}{2}\rho v_{ave}^2}, \tag{3}$$

where P_{ti} and P_{tl} are the total pressure at the inlet and the local total pressures, respectively, ρ is the fluid density, and v_{ave} is the local average velocity.

The differences observed in the casing and passage were more significant than those observed in the hub and other regions. Hence, we focused on the passage and areas near the casing, which were strongly affected by the passage and secondary flows. The reference case exhibited a weaker flow than the modified cases in the regions above the midspan. These conditions occurred because of the effects of the stator TE profile on the passage and tip leakage flow vortices. As mentioned previously, the tip leakage vortices in the TE-4 and TE-8 cases were noticeably larger than those in the reference and TE-2 cases. Therefore, there was a stronger flow in the regions above the mid-span and in the casing in the TE-4 and TE-8 cases. This phenomenon strongly affected the second stator vane's flow characteristics and heat transfer behaviour. In addition, a robust flow with a high vortex was located in the hub regions, which significantly influenced the heat transfer and fatigue life at the hub of S_2 vane, which is discussed later.

Figure 13 illustrates the flow vorticity along the S_2 axial chord length for various S_1 TE profiles. As evident, the vortex flow around the hub region was stronger than in the other regions because the total pressure loss at the hub was the lowest, as shown in Figure 12. Consequently, the heat transfer characteristics in this region increased. This phenomenon occurs because of the coupled effects of the tip leakage and casing end-wall vortices (Adams et al., 2021). In addition, the regions with a strong vortex

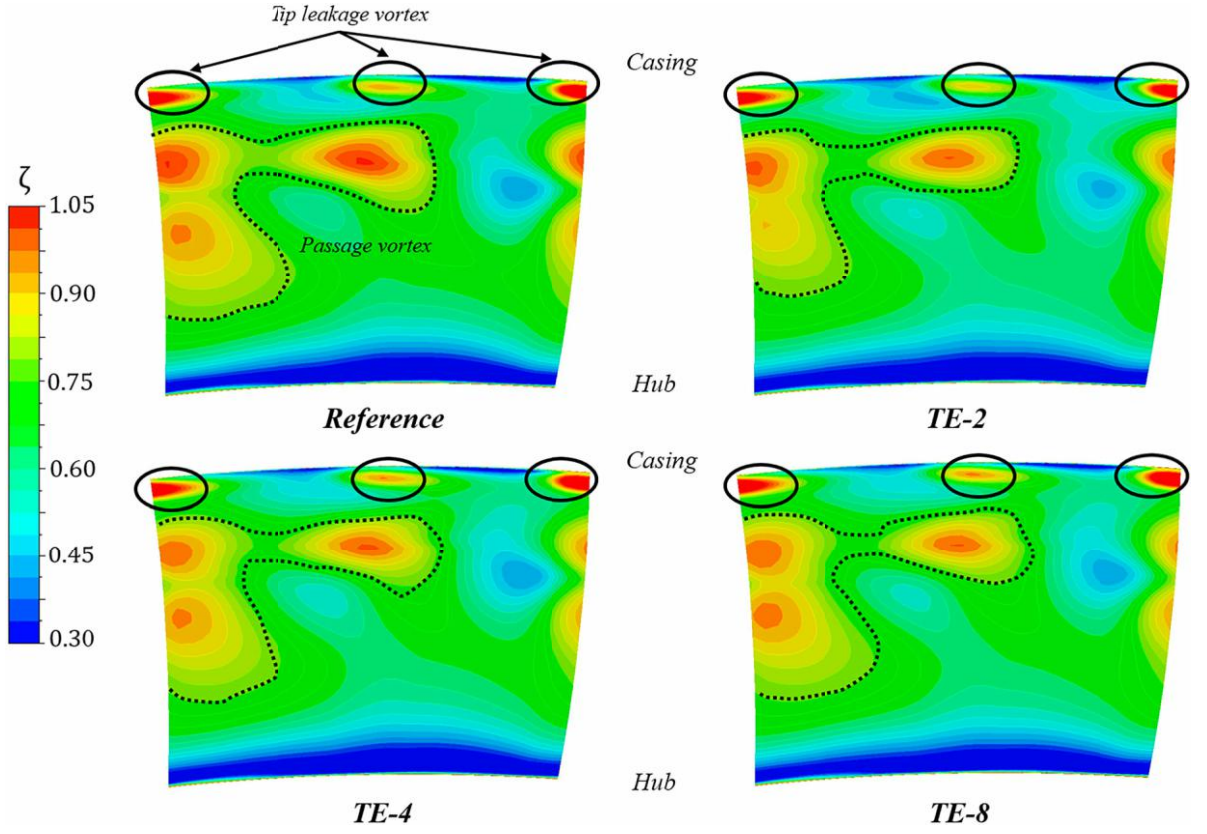

Figure 12. The contour of total pressure coefficient at entrance of the S_2 vane under various S_1 vane conditions

and high speed widened in the modified cases at 50% and 95% Ca, particularly in the region from the hub to the midspan, leading to increased temperature, heat transfer, and thermal stress in these regions. The reference case exhibited a slightly stronger vortex flow than the other modified TE cases because of the casing and hub horseshoe vortices. Overall, the downstream fluid flow characteristics were strongly affected by the TE profile of the first stator vane.

3.2. Heat transfer characteristics

Figure 14 shows the area-averaged and maximum temperature distribution on the R_1 blade and S_2 vane under various S_1 trailing-edge conditions. Both the area-averaged and maximum temperatures on the S_2 vane increased (approximately 2 K) under the modified cases compared with the reference case. By contrast, for the R_1 blade, the maximum temperature in the modified cases was higher than that in the reference case (approximately 1 K), whereas the area-averaged temperature was lower ($\sim$ 3 K). Thus, the S_1 trailing edge conditions influenced the temperature distribution on the blade and vane surface downstream, strongly affecting the heat transfer characteristics, particularly on the R_1 blade. Although the area-averaged temperature decreased, the maximum temperatures at certain positions increased. This can lead to an increase in the local heat flux as well as thermal stress, which significantly influences blade fatigue during operation.

To provide a more detailed analysis of the temperature distribution at local positions, we depicted the contour of the temperature at one of the critical positions, the hub region of the S_2 vane, as shown in Figure 15. This trend was opposite to that of the temperature distribution on the S_2 vane surface. Therefore, the temperatures of both PS and SS in the modified stator TE cases were significantly lower than those in the reference case. This degraded the heat transfer characteristics, which may decrease the thermal stress and enhance the fatigue life of the hub region. Thus, the first stator TE condition affected the fluid flow characteristics and heat transfer behaviour on the blade/vane surface downstream and in the hub region.

To evaluate the heat transfer characteristics on the blade/vane surface in various stator TE profiles, we present the dimensionless Nusselt numbers at the R_1 blade and S_2 vane, as shown in Figure 16. The Nusselt number is defined as.

$$Nu = \frac{h.Ca}{k}, \tag{4}$$

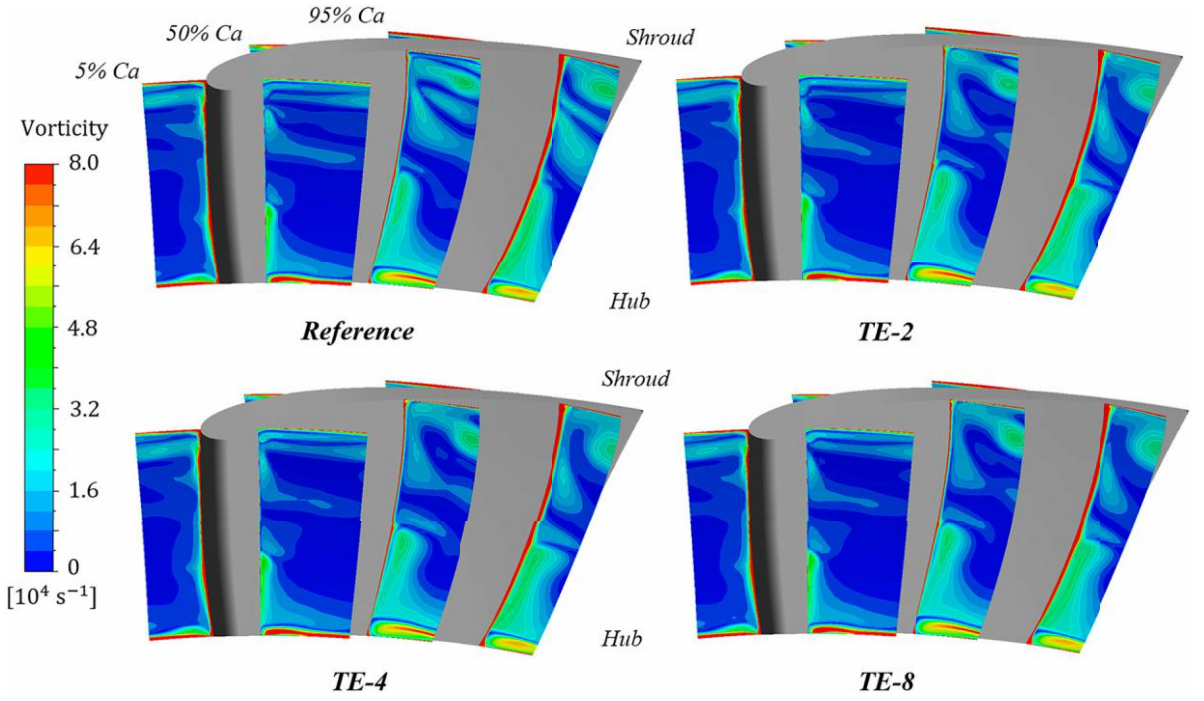

Figure 13. Contour of flow vorticity at various plane surfaces along the axial chord length of S_2 vane.

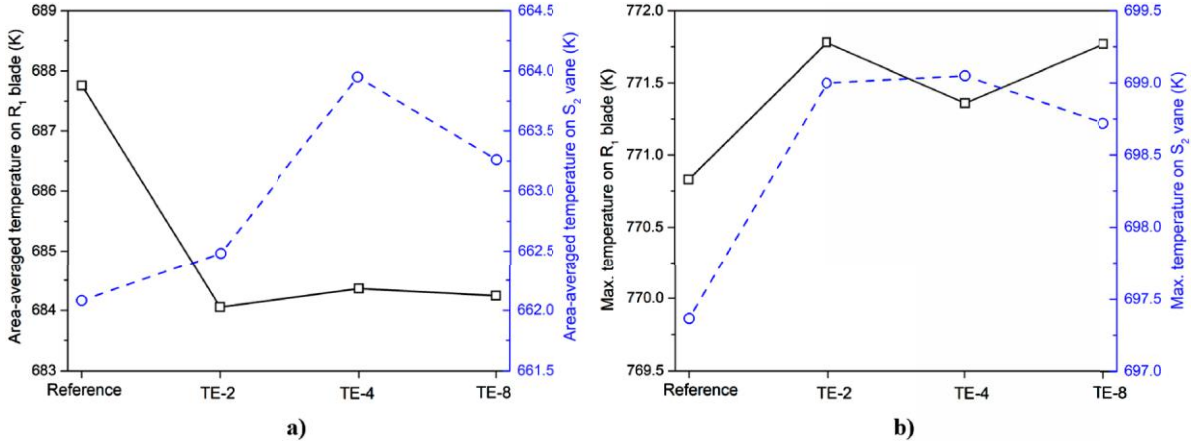

Figure 14. (a) Area-averaged temperature; (b) maximum temperature on R_1 blade and S_2 vane under various S_1 trailing-edge conditions.

where *Nu* is the nondimensional HTC (Nusselt number), *h* is the HTC on the blade/vane surface, *Ca* is the axial chord length of the blade/vane, and *k* is the fluid thermal conductivity.

Figure 16(a) shows the Nusselt number at various locations on the R_1 blade, such as the hub, shroud, and blade surfaces. The Nusselt number in the modified stator TE cases was higher than that in the reference case for all examined locations. At the hub region and blade surface, TE-4 exhibited the largest increase (approximately 0.3% and 0.2%, respectively) compared with the reference case. TE-8 exhibited a 0.9% increase in the shroud region compared with the reference case. Furthermore, at R_1, the Nusselt number in the hub region was higher than that in the shroud region (approximately 2.3%). Similarly, Figure 16(b) shows the Nusselt number in various areas of the S_2 vane. In the hub and shroud regions, the heat transfer characteristics in the modified TE cases were higher than those in the reference case, and TE-2 exhibited the largest increase (approximately 0.3% and 0.4%, respectively). Conversely, the heat transfer on the vane surface decreased in the modified cases compared to that in the reference case (approximately 0.4% in the case of TE-2). Another interesting phenomenon was that the heat transfer in the shroud region was larger than that in the hub region. In general, the first stator TE profile significantly affected the heat transfer characteristics at various locations downstream of the blade/vane.

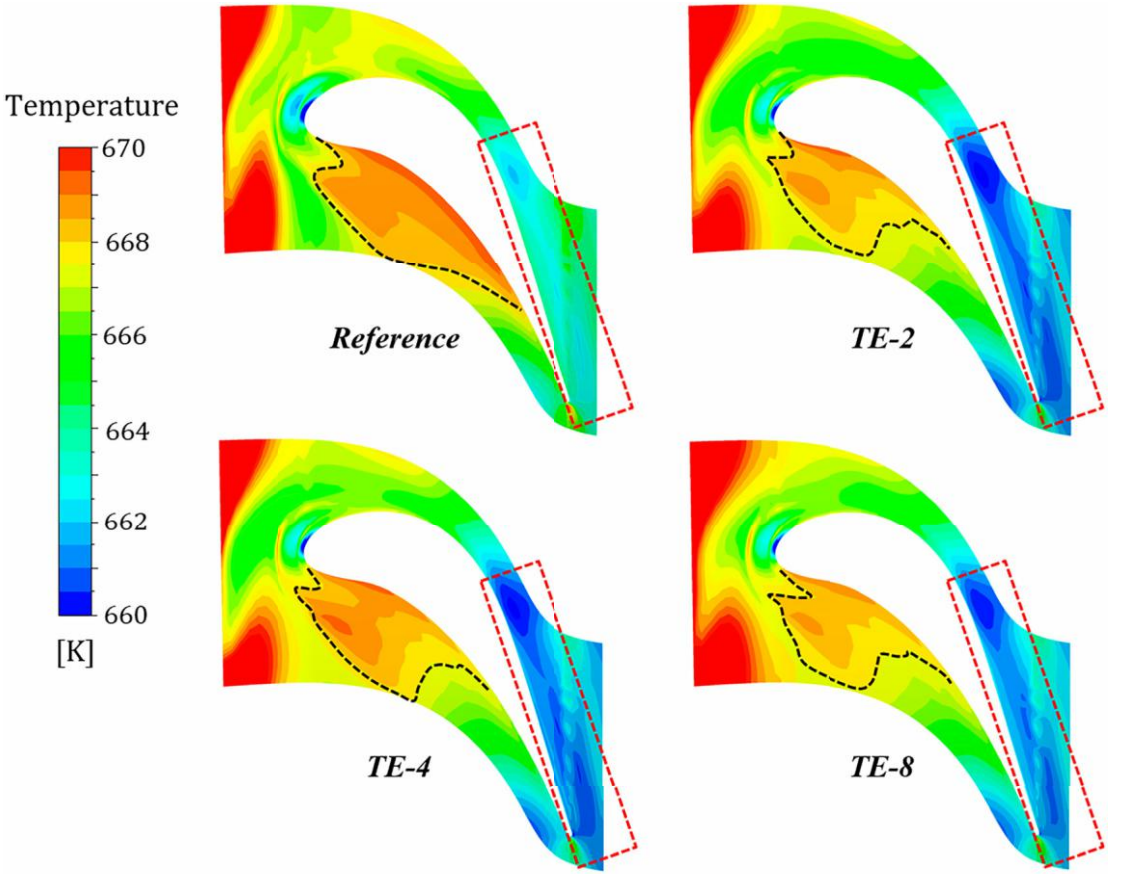

Figure 15. Contour of temperature distribution on the hub of the S_2 vane under various S_1 vane conditions.

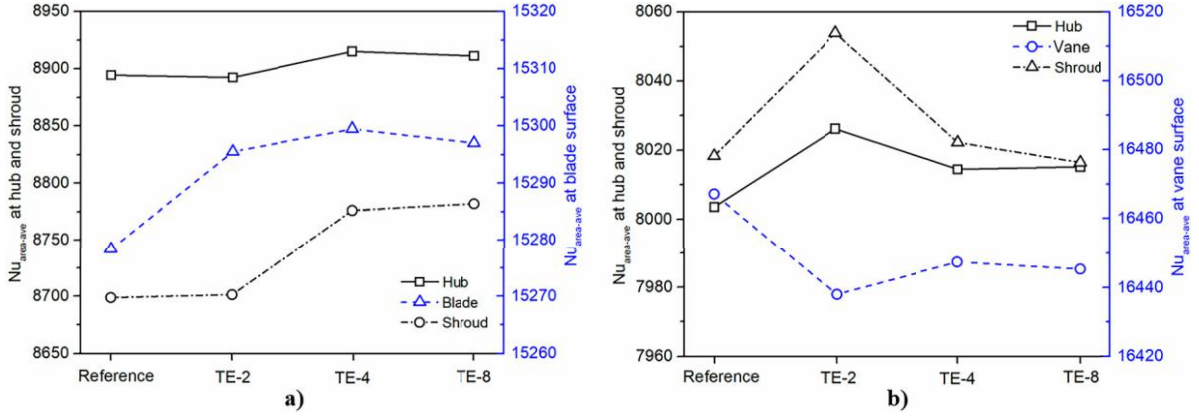

Figure 16. Area-averaged Nusselt number for various cases of S_1 vane trailing edge (TE) on the (a) R_1 blade and (b) S_2 vane.

A more detailed analysis of the heat transfer characteristics at critical locations in the blade/vane is crucial. Figure 17 shows the line plot of the heat flux distribution at the hub and shroud of the R_1 blade for various first-stator TE profiles. No difference was observed between the cases at the hub with a 70% chord length of the TE on the SS around the leading edge and the TE of the PS. This difference occurred for 20–70% of the chord length on the SS and for 25–90% of the chord length on the PS. The heat flux in the reference case was higher than in the modified stator trailing profile case. Conversely, the heat flux was similar for SS at the shroud. This difference occurred along PS, and the modified TE profile cases exported greater heat flux than the reference case. These conditions strongly affect the thermal stress in the hub and shroud regions, which may reduce the fatigue life of the rotor blades. The heat flux at the hub and shroud of the S_2 vane are shown in Figure 18. The results indicate that the effects of the first stator TE modification on the heat flux occur primarily on the SS of the

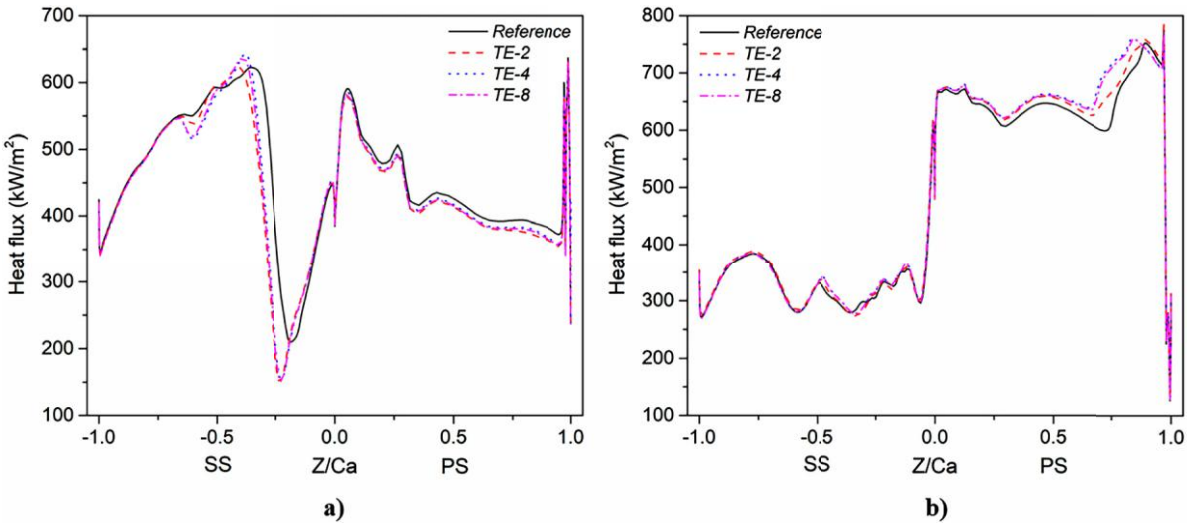

Figure 17. Heat flux distribution at (a) R_1 hub and (b) R_1 shroud under various S_1 vane conditions.

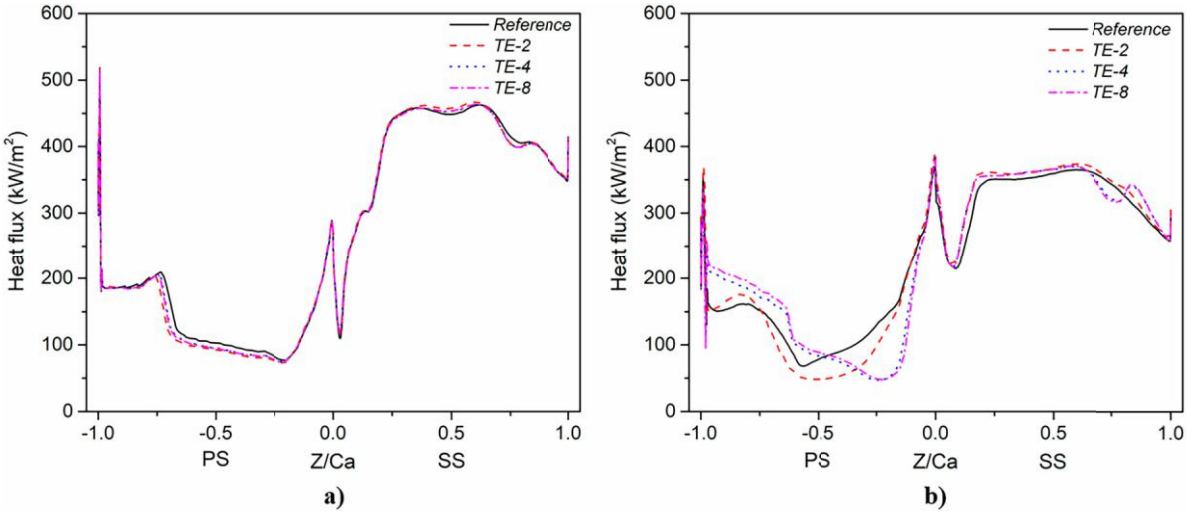

Figure 18. Heat flux distribution at (a) S_2 hub and (d) S_2 shroud under various S_1 vane conditions.

hub and PS of the shroud. These results are consistent with those of the fluid flow and temperature distribution over the blade/vane surface, as discussed above. The TE-2 case presents a significant increase compared to the other cases on the hub SS. A more complicated phenomenon occurs at the shroud. The reference case yielded a lower heat flux from 50% of the chord length of the TE on the PS; however, it increased for the region from the leading edge to 50% of the chord length on the PS. These conditions occurred because of the complex passage and secondary flows after passing through the R_1 blade, as shown in Figures 11 and 12.

3.3. Aerodynamic behaviour and overall efficiency

Figure 19(a) presents the drag and lift forces acting on the R_1 blade surface for the various analyzed cases. The modified stator TE cases exhibited significant drag and lift, whereas TE-2 exhibited the largest increases (approximately 2% and 1%, respectively) compared to the reference case. This condition is directly related to the mechanical stress on the blade surface, which strongly affects fatigue life. To explain the increase in drag and lift, the wall shear stress on the blade and vane surfaces is shown in Figure 19(b). The wall shear stress increased in the modified stator TE profile cases compared to the reference case, increasing the friction drag on the blade/vane surface. Overall, the TE condition of the first stator strongly influenced the aerodynamic characteristics of the blade/vane downstream. The overall efficiency of the turbine stage, as defined below, must be examined.

$$\eta_{oe} = \frac{h_{0,\mathrm{in}} - h_{0,\mathrm{out}}}{h_{0,\mathrm{in}} - h_{0,\mathrm{out,is}}}, \tag{5}$$

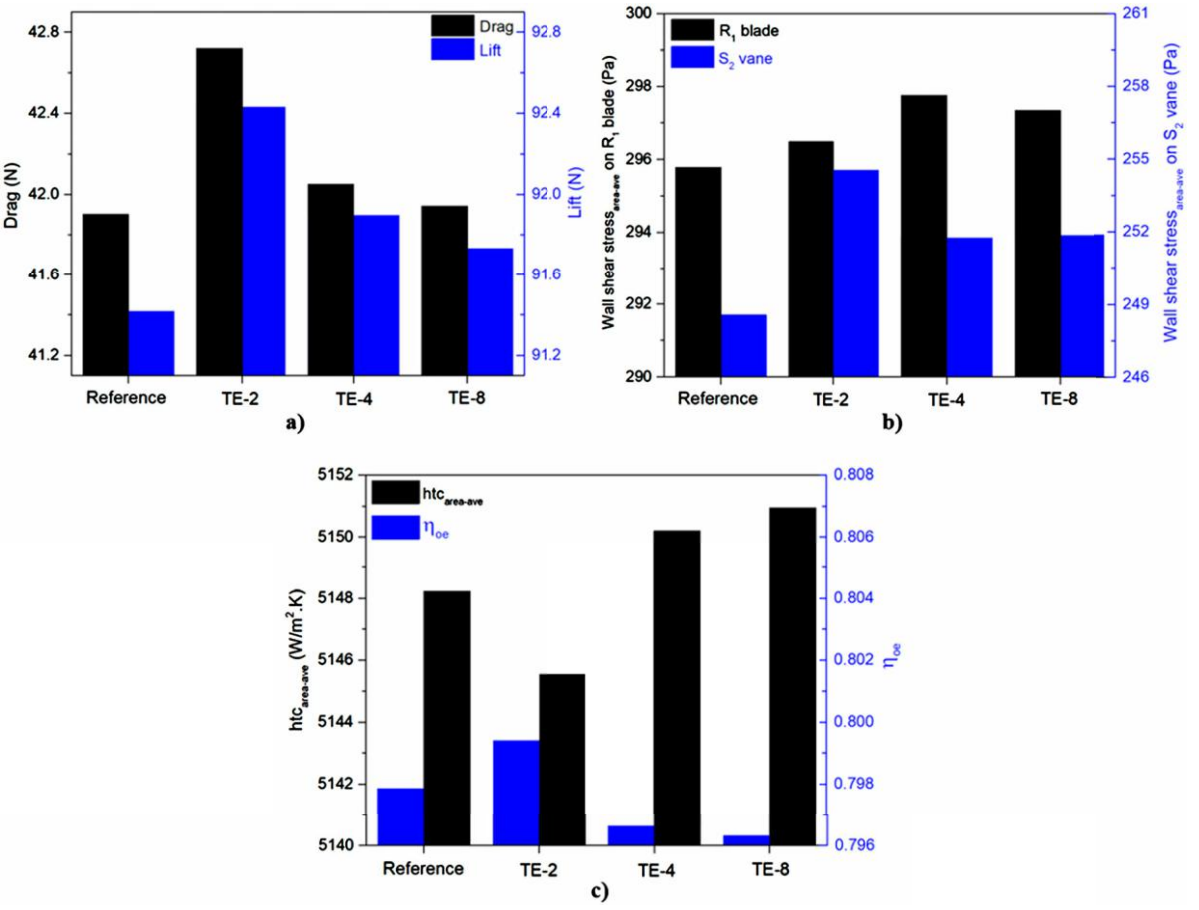

Figure 19. (a) Drag and lift forces on the R_1 blade; (b) area-averaged wall shear stress on the R_1 blade and S_2 vane; and (c) overall efficiency of turbine stage and area-averaged heat transfer coefficient (*HTC*) over the R_1 blade tip surface under various S_1 vane conditions.

where $h_{0,in}$ and $h_{0,out}$ are the total enthalpies at the inlet and outlet of the turbine stage, respectively, and $h_{0,out,is}$ is the isentropic enthalpy at the outlet following the inlet condition.

Figure 19(c) shows the overall efficiency and HTC of the rotor blade tip for various first-stator TE profiles. The overall efficiency of TE-2 was higher than that of the reference (approximately 0.15%). In contrast, the other modified profile cases demonstrated lower efficiencies than the reference case. Furthermore, the HTC on the rotor blade tip exhibited the opposite trend, with a lower HTC for TE-2 than for the reference case but a higher value for the other modified cases. These results can be explained based on the effects of tip leakage flow, which was thoroughly analyzed and discussed above. The TE-2 case had the lowest tip leakage flow and, hence, the smallest loss owing to leakage. However, more losses occurred in the TE-4 and TE-8 cases because of the higher tip leakage flow than in the reference case, resulting in lower efficiency and a higher HTC distribution on the rotor blade tip in these cases than in the reference case. Thus, the first-stator TE conditions exerted a smaller effect on the overall efficiency of the turbine stage than the heat transfer and aerodynamic characteristics.

4. Conclusions

This study conducted a numerical analysis to investigate the effects of various TE profiles of the first stator on the heat-transfer characteristics and performance in the 1.5-stage high-pressure gas turbine. Four cases were examined: a typical TE (without modification) as the reference case and three cases of modification based on the wavelength number (TE-2, TE-4, and TE-8). The results indicated an increase in the temperature and heat transfer characteristics at various locations on the blade/vane surface downstream in the modified cases compared to the reference case. This result could significantly increase the thermal stress, particularly in the hub and shroud regions. High temperatures and heat fluxes impose thermal stresses on materials, hastening fatigue mechanisms. This hastened fatigue can markedly shorten the operational life of the blades/ vanes, ultimately posing the risk of component failure. In addition, the modification of

the first-stator TE influenced the aerodynamic characteristics of the blade/vane surface. An increase (approximately 1%–2%) in the aerodynamic force (drag and lift) on the blade/vane surface in the modified cases compared with the reference case resulted in an increase in the mechanical stress, which may reduce the fatigue life of the blade/vane. Furthermore, the first stator TE profile exerted a minor effect on the gas turbine performance. The overall efficiency of the TE-2 case increased slightly (approximately 0.15%) compared to that of the reference case, whereas those of the other modified cases decreased. Thus, the modification of the first stator TE profile exerted a stronger influence on the heat transfer and aerodynamic characteristics than on the performance of the gas turbine.

This study primarily investigated the effects of various stator TE modifications on the aerodynamic characteristics, heat transfer behaviour, and performance of the gas turbine stage. Despite the significant insights gained from our study, our analysis focused primarily on flow characteristics and heat transfer phenomena without directly investigating thermal stress or fatigue life. Future research endeavours should address these aspects comprehensively. Additionally, to simplify the analysis of the hot streak, we assumed that the centre of the HS is at mid-blade height and that other regions are symmetric through the mid-span. The maximum to minimum temperature ratio was taken as 1.15, and one HS was applied to one nozzle guide vane (NGV). Furthermore, while our computational approach provides valuable insights, experimental validation would enhance the reliability and applicability of our findings. Lastly, our study pertains specifically to the conditions and configurations considered herein; thus, generalising to other turbine designs or operating conditions should be cautiously approached. Addressing these limitations will pave the way for more robust and comprehensive research in the field of gas turbine aerodynamics and thermal management.

Notations

Ca	axial chord length (mm)
K	thermal conductivity (W/m·K)
Nu	Nusselt number
P	pressure (Pa)
T	temperature (K)
PS	pressure side
SS	suction side
ζ	total pressure loss coefficient
y^+	normalised distance from the solid wall
C_p	pressure coefficient
h,	HTC heat transfer coefficient (W/m^2·K)
Ma	Mach number
TE	trailing edge
h_0	enthalpy (J/kg)
η_{oe}	overall efficiency
P_t	total pressure (Pa)
v_{ave}	local average velocity (m/s)

Disclosure statement

No potential conflict of interest was reported by the author(s).

Funding

This work was supported by the Korea Institute of Energy Technology Evaluation and Planning (KETEP) grant funded by the Korea government (MOTIE) [grant number 20193310100060], Evaluation of the performance for F-class or more gas turbine blade prototype). This work was supported by the National Research Foundation of Korea (NRF) grant funded by the Korea government (MSIT) [grant number 2022R1A5A1022977]. This work was also supported by a Korea University Grant.

Data availability statement

The data that support the findings of this study are available from the corresponding author upon reasonable request.

References

Abdelmaksoud, R., & Wang, T. (2020). Simulation of air/mist cooling in a conjugate, 3-D gas turbine vane with internal passage and external film cooling. *International Journal of Heat and Mass Transfer*, *160*, 120197. https://doi.org/10.1016/j.ijheatmasstransfer.2020.120197

Adams, M. G., Beard, P. F., Stokes, M. R., Wallin, F., Chana, K. S., & Povey, T. (2021). Effect of a combined hot-streak and swirl profile on cooled 1.5-stage turbine aerodynamics: An experimental and computational study. *Journal of Turbomachinery*, *143*(2), 021011. https://doi.org/10.1115/1.4049103

An, B.-T., Liu, J.-J., & Jiang, H.-D. (2009). Numerical investigation on unsteady effects of hot streak on flow and heat transfer in a turbine stage.

Arnone, A., & Benvenuti, E. (1994). *Three-dimensional Navier-Stokes analysis of a two-stage gas turbine (Vol. 78835)*. American Society of Mechanical Engineers.

Arnone, A., & Pacciani, R. (1996). Rotor-stator interaction analysis using the navier-stokes equations and a multigrid method.

Beard, P. F., Smith, A., & Povey, T. (2013). Impact of severe temperature distortion on turbine efficiency. *Journal of Turbomachinery*, *135*(1), 011018. https://doi.org/10.1115/1.4006389

Boyce, M. P. (2011). *Gas turbine engineering handbook*. Elsevier.

Butler, T., Sharma, O. P., Joslyn, H., & Dring, R. (1989). Redistribution of an inlet temperature distortion in an axial flow turbine stage. *Journal of propulsion and power*, *5*(1), 64–71. https://doi.org/10.2514/3.23116

Chen, W., Qiao, W., & Wei, Z. (2020). Aerodynamic performance and wake development of airfoils with wavy leading edges. *Aerospace Science and Technology*, *106*, 106216. https://doi.org/10.1016/j.ast.2020.106216

Choi, M. G., & Ryu, J. (2018). Numerical study of the axial gap and hot streak effects on thermal and flow characteristics in two-stage high pressure gas turbine. *Energies*, *11*(10), 2654. https://doi.org/10.3390/en11102654

Denton, J. D. (1993). *Loss mechanisms in turbomachines* (Vol. 78897). American Society of Mechanical Engineers.

Denton, J., & Xu, L. (1990). The trailing edge loss of transonic turbine blades.

Dorney, D. J., Davis, R. L., Edwards, D. E., & Madavan, N. K. (1992). Unsteady analysis of hot streak migration in a turbine stage. *Journal of propulsion and power*, *8*(2), 520–529. https://doi.org/10.2514/3.23507

Du, K., Li, Z., & Li, J. (2016). *Numerical investigation of the blade tip and overtip casing aerothermal performance in a high pressure turbine stage*. Turbo Expo: Power for Land, Sea, and Air.

He, L., Menshikova, V., & Haller, B. (2007). Effect of hot-streak counts on turbine blade heat load and forcing. *Journal of Propulsion and Power*, *23*(6), 1235–1241. https://doi.org/10.2514/1.29603

Hylton, L., Nirmalan, V., Sultanian, B., & Kaufman, R. (1988). *The effects of leading edge and downstream film cooling on turbine vane heat transfer*. NASA-CR-182133.

Jiang, S., Li, Z., Li, J., & Song, L. (2023). Numerical investigations on the unsteady leakage flow and heat transfer characteristics of the turbine blade squealer tip. *Journal of the Global Power and Propulsion Society*, *7*, 1–12. https://doi.org/10.33737/jgpps/157176

Jiang, Y., Wan, X., Magagnato, F., Yue, G., & Zheng, Q. (2018). Multi-step optimizations of leading edge and downstream film cooling configurations on a high pressure turbine vane. *Applied Thermal Engineering*, *134*, 203–213. https://doi.org/10.1016/j.applthermaleng.2018.02.012

Kaewbumrung, M., Tangsopa, W., & Thongsri, J. (2019). Investigation of the trailing edge modification effect on compressor blade aerodynamics using SST k-ω turbulence model. *Aerospace*, *6*(4), 48. https://doi.org/10.3390/aerospace6040048

Kerrebrock, J. L., & Mikolajczak, A. (1970). Intra-stator transport of rotor wakes and its effect on compressor performance.

Kwak, J. S., & Han, J.-C. (2003). Heat transfer coefficients on the squealer tip and near squealer tip regions of a gas turbine blade. *Journal of Heat Transfer*, *125*(4), 669–677. https://doi.org/10.1115/1.1571849

Li, Y., Su, X., & Yuan, X. (2019). The effect of mismatching between combustor and HP vanes on the aerodynamics and heat load in a 1-1/2 stages turbine. *Aerospace Science and Technology*, *86*, 78–92. https://doi.org/10.1016/j.ast.2018.12.023

Liu, J.-J., Li, P., Zhang, C., & An, B.-T. (2013). Flowfield and heat transfer past an unshrouded gas turbine blade tip with different shapes. *Journal of Thermal Science*, *22*(2), 128–134. https://doi.org/10.1007/s11630-013-0603-4

Liu, Z., Liu, Z., & Feng, Z. (2014). Unsteady analysis on the effects of tip clearance height on hot streak migration across rotor blade tip clearance. *Journal of engineering for gas turbines and power*, *136*(8), 082605. https://doi.org/10.1115/1.4026805

Liu, J., Liu, Y., He, X., & Liu, L. (2016). Study on TBCs insulation characteristics of a turbine blade under serving conditions. *Case Studies in Thermal Engineering*, *8*, 250–259. https://doi.org/10.1016/j.csite.2016.08.004

Liu, J., Liu, Y., & Liu, L. (2018). Film cooling modeling of a turbine vane with multiple configurations of holes. *Case Studies in Thermal Engineering*, *11*, 71–80. https://doi.org/10.1016/j.csite.2018.01.001

Liu, Z., Wang, Z., & Feng, Z. (2015). *Effects of inlet swirl on hot streak migration across tip clearance and heat transfer on rotor blade tip*. Turbo Expo: Power for Land, Sea, and Air.

Luo, Y., Wen, F., Wang, S., Hou, R., Wang, S., & Wang, Z. (2021). Numerical study on the biomimetic trailing edge in the environment of a high-pressure turbine stage. *Aerospace Science and Technology*, *115*, 106770. https://doi.org/10.1016/j.ast.2021.106770

Mai, T. D., & Ryu, J. (2020). Effects of Leading-Edge Modification in Damaged Rotor Blades on Aerodynamic Characteristics of High-Pressure Gas Turbine. *Mathematics*, *8*(12), 2191. https://doi.org/10.3390/math8122191

Mai, T. D., & Ryu, J. (2021). Effects of Damaged Rotor Blades on the Aerodynamic Behavior and Heat-Transfer Characteristics of High-Pressure Gas Turbines. *Mathematics*, *9*(6), 627. https://doi.org/10.3390/math9060627

Mansouri, Z. (2021). Unsteady simulation of flow and heat transfer in a transonic turbine stage under non-uniform inlet conditions. *International Communications in Heat and Mass Transfer*, *129*, 105660. https://doi.org/10.1016/j.icheatmasstransfer.2021.105660

Mishra, S., Sharma, A., & Kumari, A. (2020). Response surface methodology based optimization of air-film blade cooled gas turbine cycle for thermal performance prediction. *Applied Thermal Engineering*, *164*, 114425. https://doi.org/10.1016/j.applthermaleng.2019.114425

Pogorelov, A., Meinke, M., & Schröder, W. (2019). Large-eddy simulation of the unsteady full 3D rim seal flow in a one-stage axial-flow turbine. *Flow, Turbulence and Combustion*, *102*(1), 189–220. https://doi.org/10.1007/s10494-018-9956-9

Povey, T., Chana, K., Jones, T., & Hurrion, J. (2007). The effect of hot-streaks on HP vane surface and endwall heat transfer: An experimental and numerical study.

Povey, T., & Qureshi, I. (2009). Developments in hot-streak simulators for turbine testing.

Prapamonthon, P., Yin, B., Yang, G., & Zhang, M. (2019). Understanding of temperature and cooling effectiveness sensitivity of a film-cooled vane under coolant inlet temperature effect: A case study. *Case Studies in Thermal Engineering*, *14*, 100505. https://doi.org/10.1016/j.csite.2019.100505

Qiao, C., Li, G., Zhang, W., He, H., Duan, F., & Wang, P. (2022). Experimental study on the overall cooling effectiveness of nozzle guide vane under high temperature and high pressure. *Case Studies in Thermal Engineering*, *33*, 101923. https://doi.org/10.1016/j.csite.2022.101923

Saxer, A. P., & Giles, M. B. (1993). *Predictions of 3-D steady and unsteady inviscid transonic stator/rotor interaction with inlet radial temperature non-uniformity*. Turbo Expo: Power for Land, Sea, and Air.

Schmid, G., Krichbaum, A., Werschnik, H., & Schiffer, H.-P. (2014). *The impact of realistic inlet swirl in a 1 1/2 stage axial turbine*. Turbo Expo: Power for Land, Sea, and Air.

Simone, S., Montomoli, F., Martelli, F., Chana, K. S., Qureshi, I., & Povey, T. (2012). Analysis on the effect of a nonuniform inlet profile on heat transfer and fluid flow in turbine stages.

Timko, L. (1984). Energy efficient engine high pressure turbine component test performance report.

Vo, D.-T., Mai, T. D., Kim, B., & Ryu, J. (2022). Numerical study on the influence of coolant temperature, pressure, and thermal barrier coating thickness on heat transfer in high-pressure blades. *International Journal of Heat and Mass Transfer*, *189*, 122715. https://doi.org/10.1016/j.ijheatmasstransfer.2022.122715

Wang, Z., Liu, Z., & Feng, Z. (2016). Influence of mainstream turbulence intensity on heat transfer characteristics of a high pressure turbine stage with inlet hot streak. *Journal of Turbomachinery*, *138*(4), 041005. https://doi.org/10.1115/1.4032062

Wang, Z., Wang, D., Liu, Z., & Feng, Z. (2017). Numerical analysis on effects of inlet pressure and temperature nonuniformities on aero-thermal performance of a HP turbine. *International Journal of Heat and Mass Transfer*, *104*, 83–97. https://doi.org/10.1016/j.ijheatmasstransfer.2016.08.018

Wang, Z., Wang, D., Wang, Z., & Feng, Z. (2018). Heat transfer analyses of film-cooled HP turbine vane considering effects of swirl and hot streak. *Applied Thermal Engineering*, *142*, 815–829. https://doi.org/10.1016/j.applthermaleng.2018.07.044

Wu, Z., Zhu, H.-R., Li, L., Xu, Z.-P., & Zhang, Z. (2022). Experimental study of the effect of swirling inflow on film cooling effectiveness. *Case Studies in Thermal Engineering*, *32*, 101871. https://doi.org/10.1016/j.csite.2022.101871

Xu, Q., Du, Q., Wang, P., Liu, J., & Liu, G. (2018). Computational investigation of film cooling and secondary flow on turbine endwall with coolant injection from upstream interrupted slot. *International Journal of Heat and Mass Transfer*, *123*, 285–296. https://doi.org/10.1016/j.ijheatmasstransfer.2018.01.117

Yan, Y., Avital, E., Williams, J., & Cui, J. (2021). Aerodynamic performance improvements of a vertical axis wind turbine by leading-edge protuberance. *Journal of Wind Engineering and Industrial Aerodynamics*, *211*, 104535. https://doi.org/10.1016/j.jweia.2021.104535

Yao, C.-Y., Zhang, Z., Zhang, B.-L., & Zhu, H.-R. (2021). Heat transfer characteristic of a fully cooled turbine vane. *Case Studies in Thermal Engineering*, *28*, 101547. https://doi.org/10.1016/j.csite.2021.101547

Zeng, L., Chen, P., Li, X., Ren, J., & Jiang, H. (2018). Influence of simplifications of blade in gas turbine on film cooling performance. *Applied Thermal Engineering*, *128*, 877–886. https://doi.org/10.1016/j.applthermaleng.2017.09.008

Zhang, B., & Qiang, X. (2021). Aerothermal and aerodynamic performance of turbine blade squealer tip under the influence of guide vane passing wake. *Proceedings of the Institution of Mechanical Engineers, Part A: Journal of Power and Energy*, *235*(4), 651–670. https://doi.org/10.1177/0957650920965733

Zhang, B., Qiang, X., Lu, S., & Teng, J. (2020). Numerical investigations of unsteady passing wake effects on turbine blade tip aerothermal performance with different tip clearances. *International Journal of Numerical Methods for Heat & Fluid Flow*, *30*(2), 792–817. https://doi.org/10.1108/HFF-05-2019-0411

Zhang, B., Qiang, X., Teng, J., & Lu, S. (2019). *Unsteady passing wake effects on turbine blade tip aerodynamic and aerothermal performance with film cooling*. Turbo Expo: Power for Land, Sea, and Air.

Zhang, S., Shuiting, D., Peng, L., & Tian, Q. (2023). Effects of swirl and hot streak on thermal performances of a high-pressure turbine. *Chinese Journal of Aeronautics*, *36*(5), 250–267. doi:10.1016/j.cja.2023.03.052